(Received 17 June 2024, Accepted 4 August 2024, Scheduled 19 September 2024)

Investigation of Stator/Rotor Pole Number Combinations and PM Numbers on Variable Flux Leakage PM Machine

Xiping Liu, Ruipan Lu, Yuxin Liu, and Wenrui Wang*

School of Electrical Engineering and Automation, Jiangxi University of Science and Technology, Ganzhou 341000, Jiangxi, China

ABSTRACT: This paper proposes a variable flux leakage permanent magnet (PM) machine and investigates the impact of slot and pole number combinations on the electromagnetic performance of a variable flux leakage permanent magnet machine (VFL-PMM). The stator armature winding *dq*-axis magnetic circuit is designed to couple with the PM leakage magnetic circuit by the deliberate establishment of a leakage-guided magnetic barrier and a poly-magnetic barrier on the rotor side. The VFL-PMM with 12s10p-DL (double layers) fractional slot centralized winding (FSCW) serves as an illustrative example of global parametric modelling of the machine. The objective is to optimize the split ratio, average torque, torque ripple, and PM utilization of the machine to obtain the optimum amount of the machine. The relationship between the no-load, on-load characteristics, and variable flux leakage characteristics of 12s8p, 12s10p, 12s14p with double-layer FSCW and 12s10p with single-layer FSCW are studied comparatively. The machines are analyzed and optimized using 2D finite element analysis.

1. INTRODUCTION

Interior permanent magnet synchronous machine (IPMSM) is a highly versatile component that finds application in a multitude of industrial contexts, primarily due to its superior power density, efficiency, and power factor, which are particularly advantageous in the electric vehicle industry [1–3]. Electric machine-based drive systems serve as crucial components of electric vehicles and represent a significant embodiment of their core competitiveness [4–6]. However, when facing increasingly complex traffic conditions such as frequent starting and stopping, acceleration and deceleration, hill climbing and high-speed cruising, higher demands are placed on the machine's speed range, operating efficiency, and operating modes. In contrast to traditional permanent magnet machines whose working point is essentially fixed, it is difficult to adjust the narrow speed range of variable magnetic field machines which results in low efficiency and limited operation modes [7–10]. The variable flux leakage permanent magnet machine is designed to adjust the magnitude of the leakage flux of the permanent magnet tangentially by adjusting the magnitudes of both the armature current and magnetic barrier in the q-axis. This enables precise control over the magnitude of the leakage flux caused by additional magnetic barriers, thus achieving the characteristic of adjustable air-gap flux. In contrast to conventional machines, which consider flux leakage as a loss, variable leakage machines utilise both inter-polar leakage and self-leakage effectively. The inter-pole leakage can be controlled by segmenting the permanent magnet (PM) and designing the magnetic barrier in the q-axis, thus achieving regulation of the main magnetic circuit.

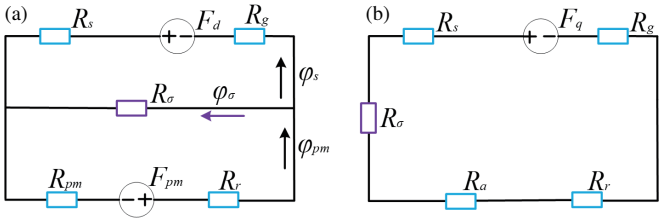

FIGURE 1. d-axis equivalent magnetic circuit. (a) VFL-PMM. (b) Conventional PMM.

The d-axis equivalent circuit models of the VFL-PMM and conventional PMM are depicted in Fig. 1. By adjusting the current, the strength of the rotor-generated magnetic field can be controlled, thereby influencing the d-axis motive force (MMF) and enabling a wider speed regulation range for the machine. The VFL-PMM was initially proposed by Kato's team in 2013 [11, 12]. It is designed with two layers of air barrier at the ends of permanent magnets to form a leakage circuit within the rotor core. In the absence of a load, the leakage flux increases, thereby reducing the main flux. Conversely, during load operation, the larger armature current alters the magnetic saturation extent of the rotor core, suppressing the leakage flux and increasing the main flux. The conventional design concept of reducing leakage flux in PMSM is challenged by the innovative VFL-PMM, which introduces a leakage bypass with adjustable flux density. By controlling the armature current, the air gap can be adjusted to regulate the amount of leakage flux. Previous studies [13–17] have proposed curved and elliptical magnetic barriers to form a leakage circuit on a conventional PMSM rotor structure. Part of the machine's flux is guided through the mechanism magnetic bridge and magnetic barrier to create inter-pole leakage under specific

* Corresponding author: Wenrui Wang (wwr1306543853@gmail.com).

conditions. It has been investigated that the extent of leakage circuit acceleration in VFL-PMM type can be controlled through armature current, indirectly regulating the amount of maximum leakage flux. This enables wide speed regulation and improved operating efficiency within different working regions.

However, the torque density of the VFL-PMIM is relatively small compared to that of a conventional permanent magnet machine. Furthermore, a reduction in power factor is observed as a consequence of the high flux armature field and flux leakage. From a theoretical standpoint, a diminished power factor is inherently linked to the inductance parameters. In general, conventional permanent magnet machines exhibit a reduction in flux-weakening capability due to the weakening of their d-axis inductances. Furthermore, the distinction in dq-axis inductance can be elucidated through the lens of reluctance torque. While augmenting the prominence ratio of the motor can effectively enhance the reluctance torque, the limit of L_d will be constrained due to the saturation of the motor core. It is usually required to enhance the reluctance torque in order to expand the constant power speed range of the machine. However, for conventional interior permanent magnet structures, this would necessitate an increase in inverter capacity, resulting in reduced efficiency and power factor of the drive system. Additionally, there is a risk of irreversible demagnetization of the magnets due to negative d-axis current generating opposing polarity armature reaction flux on the permanent magnets. In the design of variable-leakage-flux machines, researchers influence the inductance through the interaction of pole-slot combinations to improve the efficiency of the machine for practical applications. Specifically, VFL-PMM differs from PMSM due to its lower torque density, which poses a major constraint for practical implementations. Therefore, the investigation of slot and pole combinations with high torque density and wide speed-range is of significant practical importance in the study of permanent magnet machines. In [18], the focus is on examining the impact of slot-pole configurations on the overall performance of AFPM machines equipped with ironless stator windings. The concept of magnetic field localization is defined and derived through an analysis of copper consumption and utilization at different slot numbers and stator diameters. Additionally, the characteristics of cogging torque are analyzed for permanent magnet double rotor structures with varying numbers of poles. In [19], a new type of three-phase stator hybrid excited machine with permanent magnets (PMs) located at the slot openings of field winding slots is introduced. The open-circuit and load characteristics of machines with different slot and pole combinations as well as the effects of DC current and the unbalanced magnetic force are investigated comparatively. In [20], pole-slot combinations based on balanced conditions are summarized to provide general guidance for constructing new multi-tooth modulated machines. Ref. [21] investigates the influence of stator and rotor pole numbers combinations and permanent magnet numbers on electromagnetic performance of consequent-pole hybrid excited flux reversal machines. Global optimization is performed to obtain the optimal combination of rotor and stator pole number and the optimal number of permanent magnets for maximum average torque without limiting the permanent magnet volume. The corresponding cogging torque, average torque, torque fluctuation, inductance, unbalanced magnetic pull, and flux regulation capabilities are compared. A symmetric FSCW with a multi-layer structure with unconventional slot and pole combinations is proposed in [22]. The performances of conventional and unconventional slot and pole combinations are compared in terms of winding coefficients, rotor eddy current losses, cogging torque, and eccentricity-free radial force through finite element simulation. The results demonstrate that the conventional and unconventional pole-slot combinations are consistent in all aspects.

The paper is organized as follows. First, the slot and pole combinations of the VFL-PMM and the operating principle of variable leakage are introduced. Then, the VFL-PMM with a fractional slot concentrated winding (1210p-DL) is selected as an example for the parametric modelling of the machine. Finally, optimization is performed to improve the split ratio, average torque, torque ripple, and PM utilization of the machine. The electromagnetic performance is analyzed for different slot and pole combinations, including cogging torque, average torque, torque ripple, inductance, variable flux leakage characteristics, and efficiency.

2. MACHINE TOPOLOGIES

The conventional machines typically feature a magnet barrier deeply implanted at the end of the permanent magnet in order to enhance its magnetic flux. However, the high reluctance of this barrier hinders speed regulation of the machine. The slot and pole combination topologies of the VFL-PMM are illustrated in Fig. 2, depicting a 12s10p double-layer FSCW, a 12s10p single-layer FSCW, and a 12s14p double-layer FSCW, respectively. The PMs have a "V" structure with two leakage bypasses between neighboring PMs. The main magnetic barrier is located at the end of the PM and close to the air gap, and the curved magnetic barrier between neighboring PMs is the secondary magnetic barrier. The purpose of setting these two magnetic barriers is to reduce the q-axis inductance to a certain extent.

Based on the above analysis, this paper will comprehensively consider the machine magnetic motive force harmonic content, winding coefficients, torque density, and flux-weakening in order to meet the requirement of high reliability under multiple operating conditions. Different slot and pole combinations produce different d-axis inductances, which in turn produce d-axis armature reactance, which plays a major role in the flux-weakening characteristics in PMSM.

According to [23], VFL-PMMs with FSCW having balanced phase windings can be classified into different N_{sp}

$$N_{sp} = GCD(N_s, p)/v \tag{1}$$

where N_s is the slot number; p is the pole-pair number; v is 1 or 2 for double-layer (DL) or single-layer (SL) windings; GCD (N_s, p) is the greatest comment divisor of N_s and p. The VFL-PMM with FSCW can be divided into two groups according to the number of coils of one phase in one machine. Equation (2)

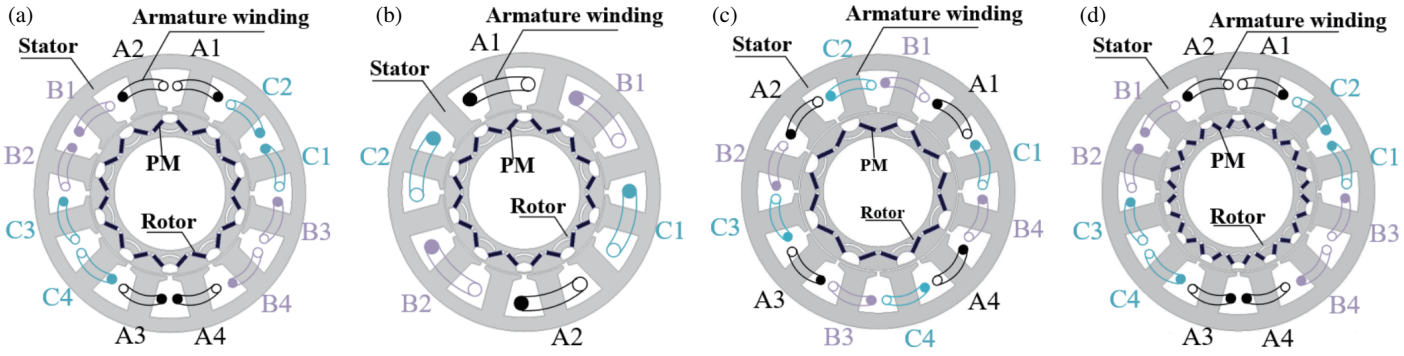

FIGURE 2. Slot and pole combination for VFL-PMM topologies. (a) 12s10p-DL. (b) 12s10p-SL. (c) 12s8p-DL. (d) 12s14p-DL.

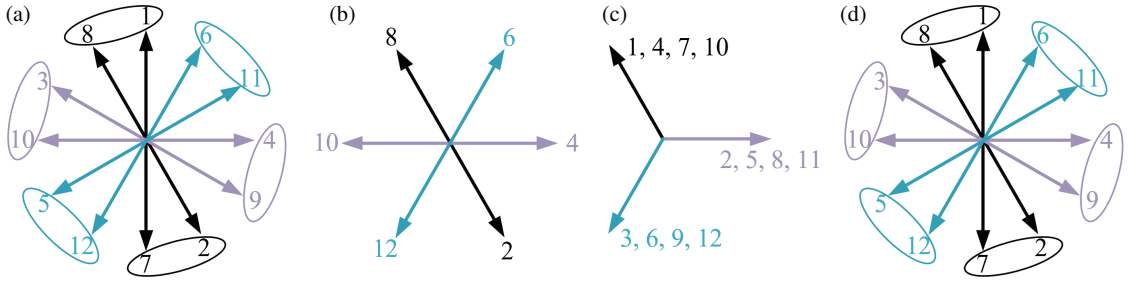

FIGURE 3. Coil flux phasor diagrams of different armature winding poles. (a) 12s10p-DL. (b) 12s10p-SL. (c) 12s8p-DL. (d) 12s14p-DL.

is odd, and Equation (3) is even.

$$\frac{N_s}{mGCD(N_s,p)} = 2k-1, \quad (k=1,2,3\ldots) \tag{2}$$

$$\frac{N_s}{mGCD(N_s,p)} = 2k, \quad (k=1,2,3\ldots) \tag{3}$$

For three-phase VFL-PMM with FSCW ($m = 3$), the VFL-PMMs with 12s10p-DL ($N_{sp} = 1$), 12s10p-SL (N_{sp} =1), and 12s14p-DL (N_{sp} =1) belong to Equation (2). On the other hand, for three-phase VFL-PMM with FSCW ($m = 3$), the VFL-PMM with 12s8p-DL (N_{sp} =4) shown in Fig. 2(c) belongs to Equation (3). The back-EMF vectors distributions of slot conductors for 12s10p-DL, 12s10p-SL, 12s8p-DL, 12s14p-DL are shown in Fig. 3.

3. OPTIMIZATION

Taking 12s10p-DL as an example, the effects of stator and rotor parameters on the electromagnetic performance of VFM-PMM are investigated, including average torque, torque fluctuation, PM consumption, iron loss, and efficiency.

The tooth width of the stator is T_w, and the slot depth is S_d. The split ratio is a parameter for optimizing the stator and can be defined as

$$\lambda = \frac{D_i}{D_o} \tag{4}$$

where D_o and D_i are the outer radius and inner radius of the stator, respectively.

The saturation of the stator core and the armature reaction act as a limiting factor in the potential for the further improvement of the machine's output torque. Consequently, the impact of the stator split ratio on the machine's output torque is examined, beginning with an analysis of the structural parameters. The specific structural parameters are shown in Table 1.

TABLE 1. Basic Design Specifications Of VFL-PMM.

Parameter	Unit	Value
Out radius of stator	mm	150
Out radius of rotor	mm	87.8
Stack length of the machine	mm	80
Rated voltage	V	120
Rated speed	r/min	1500
Pole slot combination	–	10/12
Number of turns	–	20
Air-gap length	mm	0.7
Rated power	Kw	2.5
Current density	A/mm^2	5
Length of magnet	mm	9

When the stator outer diameter is unchanged, the larger the stator split ratio is, the larger the stator slot area and tooth area are, and the output torque can be increased by increasing the electrical load. When the stator split ratio is small, the rotor outer diameter becomes larger; the air gap magnetic density increases; and the output torque can be increased by the increase of magnetic load.

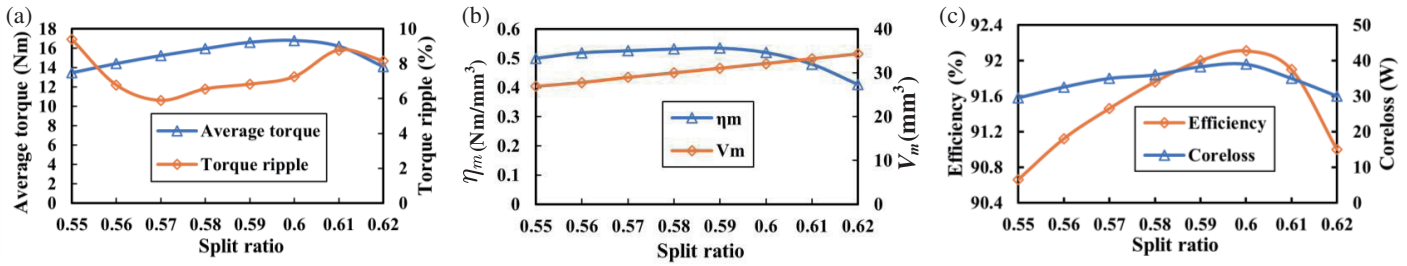

FIGURE 4. Variations of average torque, torque ripple, PM utilization ratio and iron loss, efficiency with split ratio in 12s10p-DL. (a) Average torque and torque ripple. (b) PM volume V_m and PM utilization ratio. (c) Core loss and efficiency.

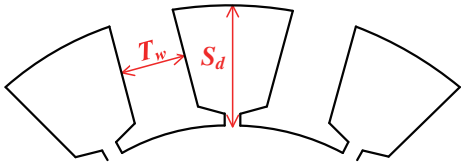

FIGURE 5. Optimized structural parameters of stator.

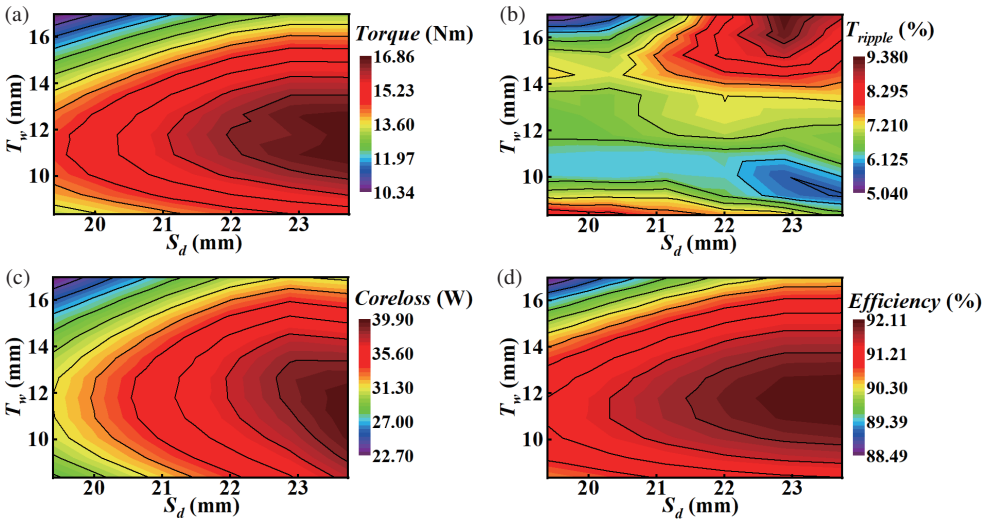

FIGURE 6. Variations of average torque, torque ripple, core loss, efficiency with tooth width and slot depth in 12s10p-DL. (a) Average torque (b) torque ripple. (c) Core loss (d) efficiency.

Figure 4 demonstrates the variations of average torque, torque ripple, PM utilization ratio, and iron loss, efficiency with split ratio in 12s10p-DL VFL-PMM. From the plot it can be seen that the point of maximum torque is at split ratio = 0.6, while the point of minimum torque fluctuation is at split ratio = 0.57. The maximum point of PM utilization is at split ratio = 0.59, and at split ratio = 0.6 the PM utilization starts to decrease. As can be seen in Fig. 3(c), the points of the highest iron consumption and efficiency are both at split ratio = 0.6. The optimized parameters of the stator structure are shown in Fig. 5.

Figures 6(a) and (b) demonstrate the variation of average torque and torque ripple with tooth width and slot depth in VFL-PMM with 12s10p-DL. It was observed that the average torque increased with increasing slot depth, while the torque ripple exhibited a decrease with increasing slot depth. The tooth width exhibits larger torque and smaller torque ripple in the range of 10 mm–12 mm. Figs. 6(c) and (d) illustrate the variation patterns of core loss and efficiency with tooth width and slot depth in the VFL-PMM with 12s10p-DL. It is observed that both core loss and efficiency increase with increasing tooth width and slot depth.

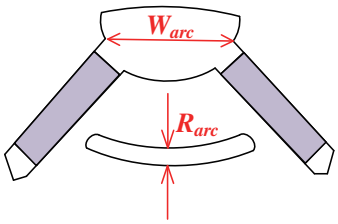

FIGURE 7. Optimized structural parameters of magnetic barrier.

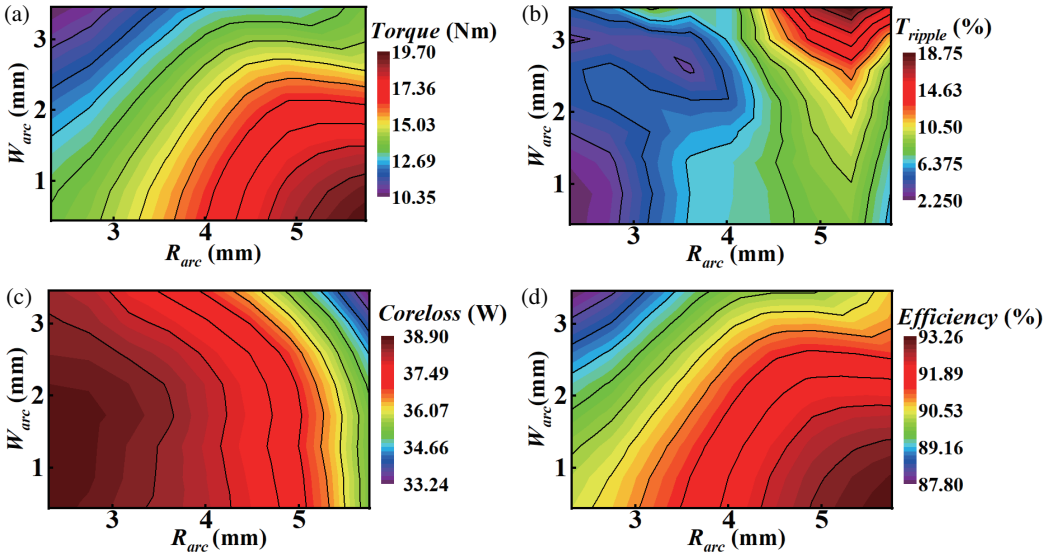

FIGURE 8. Variations of average torque, torque ripple, core loss, efficiency with flux barriers in 12s10p-DL. (a) Average torque, (b) torque ripple, (c) core loss, (d) efficiency.

The parameters of the rotor magnetic barrier are shown in Fig. 7 for optimizing the width of the rotor magnetic barrier. Figs. 8(a) and (b) demonstrate the variation of the average torque and torque fluctuation with the width of the magnetic barrier in the VFL-PMM with 12s10p-DL. It can be observed that an increase in R_{arc} and a decrease in W_{arc} result in a notable enhancement in the average torque of the VFL-PMM. Consequently, the torque ripple of the VFL-PMM is observed to diminish in conjunction with an increase in the width of the magnetic barriers. Figs. 8(c) and (d) demonstrate the variation patterns of the average torque and torque fluctuation with the width of the magnetic barrier in the VFL-PMM with 12s10p-DL. It can be seen that the rotor iron consumption decreases with the increase of R_{arc} and W_{arc}. The variation of efficiency is similar to the corresponding average torque. As mentioned above, the magnetic barrier can improve the unbalanced magnetic flux, thus reducing the core loss and increasing the average torque and efficiency.

4. ELECTROMAGNETIC PERFORMANCES

This section presents a comparative analysis of the electromagnetic performance of the final optimized VFL-PMM slot-pole combination structure, with the objective of identifying the optimal VFL-PMM slot and pole combinations. The cross-sections of the final optimized designs of the four machines are illustrated in Figs. 9(a), (b), (c), (d), together with their open-circuit flux density and flux line distribution.

4.1. Open-Circuit Characteristics

The open-circuit back-EMFs with different slot and pole combinations are compared in Fig. 10. In particular, the back-EMF amplitude of 12s8p-DL is the largest, and the back-EMF amplitude of 12s14p-DL is the smallest. In order to quantitatively analyze the opencircuit back-EMF harmonics, the total harmonics distortion (THD) of the opencircuit back-EMF was calculated according to Equation (5).

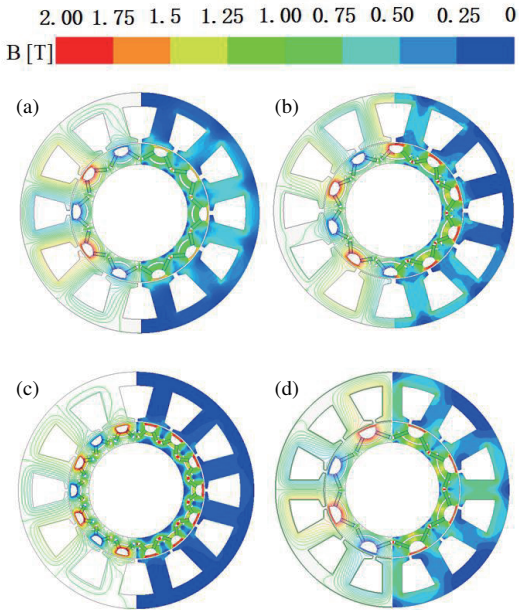

FIGURE 9. Field distributions at open-circuit with different slot/pole combinations. (a) 12s10p-DL. (b) 12s10p-SL. (c) 12s14p-DL. (d) 12s8p-DL.

$$\text{THD} = \frac{\sqrt{\left|\sum_{n=1}^{10} E_{cv}^2 - E_{c1}^2\right|}}{E_{c1}} \tag{5}$$

where E_{cv} is the amplitude of the vth harmonic back EMF, and E_{c1} is the amplitude of the fundamental back EMF.

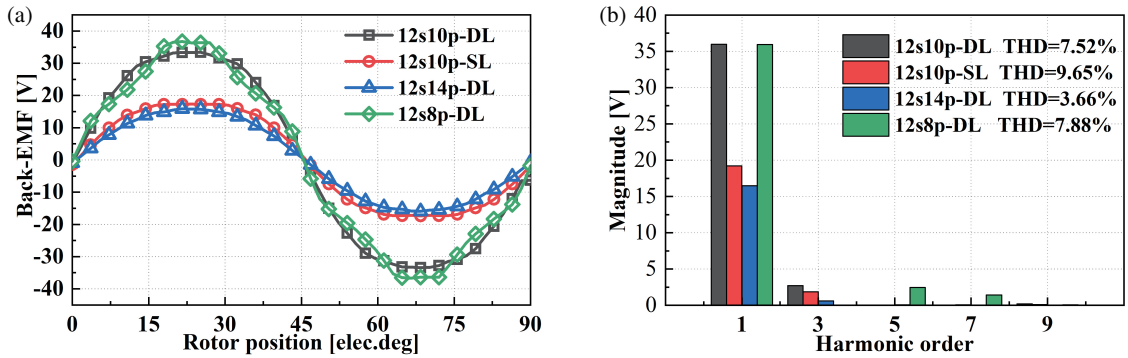

FIGURE 10. Phase back-EMFs of VFL-PMM's slot and pole combinations. (a) Waveforms. (b) Harmonics. (1500 r/min).

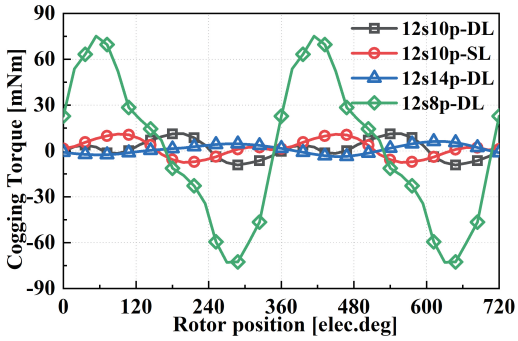

FIGURE 11. Variable of cogging torques with different slot and pole combinations.

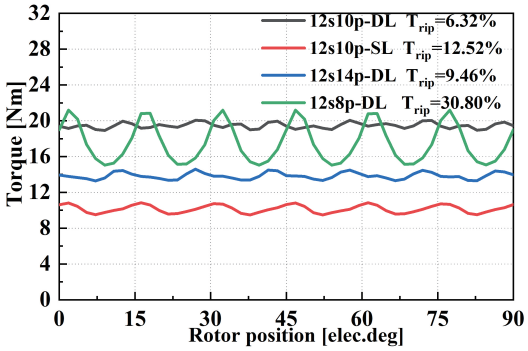

FIGURE 12. Variable of electromagnetic torque with different slot and pole combinations.

It can be observed that 12s14p-DL has the lowest harmonic distortion rate, which indicates that the larger the number of poles is, the lower the harmonic content of the machine is. The back-EMF harmonic content of the 12s14p-DL VFL-PMM is significantly lower than that of the 12s8p-DL VFL-PMM.

The no-load torque is generated by the radial force component that is produced between the stator and rotor teeth when the stator windings are not energized. The open circuit torque T_{cog} can be defined as the negative derivative of the magnetic field energy W, which is produced by the unenergized stator windings, with respect to the angular position α of the stator and rotor.

$$T_{cog} = 1\frac{\partial W}{\partial \alpha} \tag{6}$$

Given the significant impact of slot opening width on cogging torque, a consistent slot opening width is selected for comparative analysis of the four machines. The cogging torque waveforms for these four types of slot-pole combinations obtained by finite element analysis are shown in Fig. 11. It can be observed that the cogging torque of 12s8p-DL is the highest, and the cogging torque of 12s14p-DL is the lowest among these four types of slot and pole combinations.

4.2. Electromagnetic Torque

The variations of the electromagnetic torques of all the machines are illustrated in Fig. 12. T_{avg} is the average torque; T_{peak} is the peak torque; and $T_{\min}$ is the minimum torque. T_{rip} is the torque ripple defined as

$$T_{rip} = \frac{T_{peak} - T_{\min}}{T_{avg}} \times 100\% \tag{7}$$

It can be seen that 12s10p-DL has the largest average torque, while 12s10p-SL has the smallest average torque. It can also be seen that the torque ripple of 12s8p is the largest, and the torque ripple of 12s14p-DL is slightly larger than that of 12s10p-SL, which is roughly the same as the above-mentioned case of cogging torque.

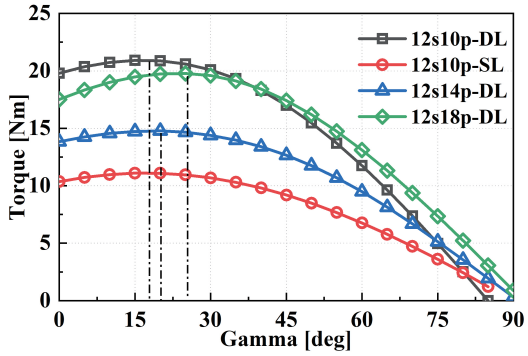

FIGURE 13. Waveforms of torques with current angle.

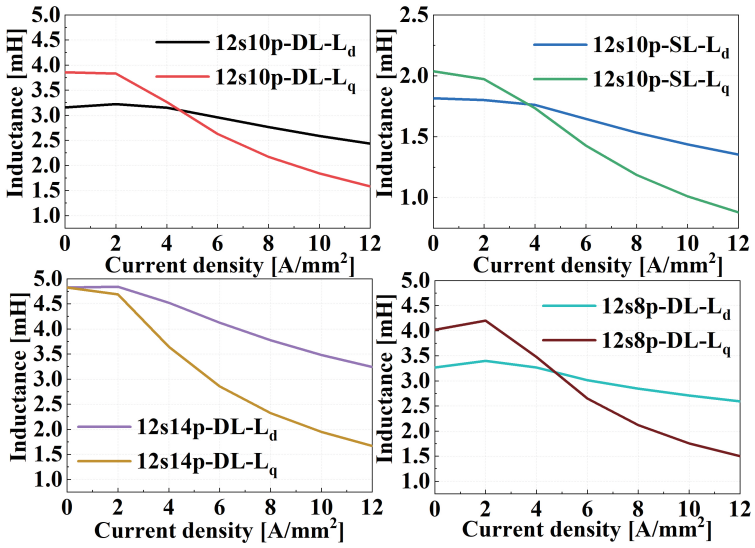

FIGURE 14. Waveforms of dq-axis with different current density.

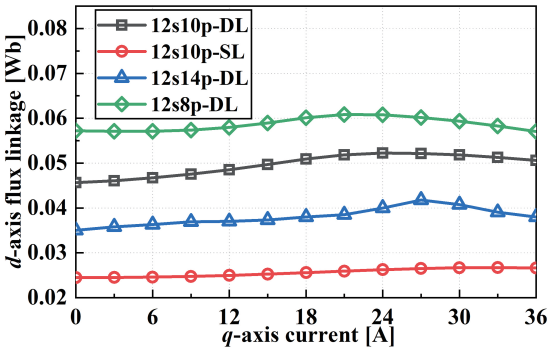

FIGURE 15. The variable curve of d-axis flux linkage with q-axis current.

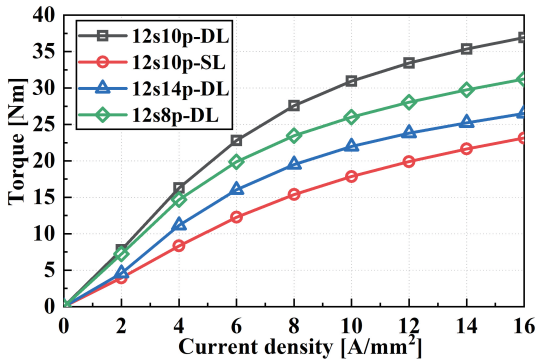

FIGURE 16. The variable curve of torque with current density.

Figure 13 depicts the torque variation of the four machines at different current angles from 0 to 90°. With the same number of permanent magnets, it can be seen that the highest torque point is at 15° current angle from 12s10p-DL. The current angle of the highest torque point for all motors is greater than 0, which also reflects the side effect that the reluctance torque is negligible, and the difference between the dq-axis inductance is less obvious.

4.3. Inductance Characteristic

The variation curves of the dq-axis inductance at different current densities are depicted in Fig. 14. Basically, L_d is greater than L_q at rated operating conditions.

The graph demonstrates the variation in the saliency ratio of the four machines under different operating conditions, presented in a side-by-side comparison. L_d decreases slower than L_q for all machines, which is due to the presence of the q-axis magnetic barrier leading to the increase of the inter-pole leakage flux. Due to the low reluctance of the leakage circuit, both the armature flux and leakage flux will preferentially pass through the leakage circuit. So q-axis inductance L_q will go down faster than d-axis inductance L_d.

4.4. Variable Flux Leakage Property

In order to validate the variable flux leakage property of the VFL-PMM, Fig. 15 illustrates the variation curve of the d-axis flux linkage with the q-axis current for each machine. The variable flux rates for 12s10p-DL, 12s10p-SL, 12s14p-DL, and 12s8p-DL are 16.22%, 8.3%, 6.3%, and 8.3%, respectively. Under open-circuit condition, all machines show more obvious flux leakage state. With the increase of armature current, the saturation state of the leakage bypass region gradually increases, leading to the decrease of leakage flux and increase of the main PM flux linkage.

4.5. Overload capability

The electromagnetic torque versus electrical density for the slot and pole combinations of the VFL-PMM is shown in Fig. 16.

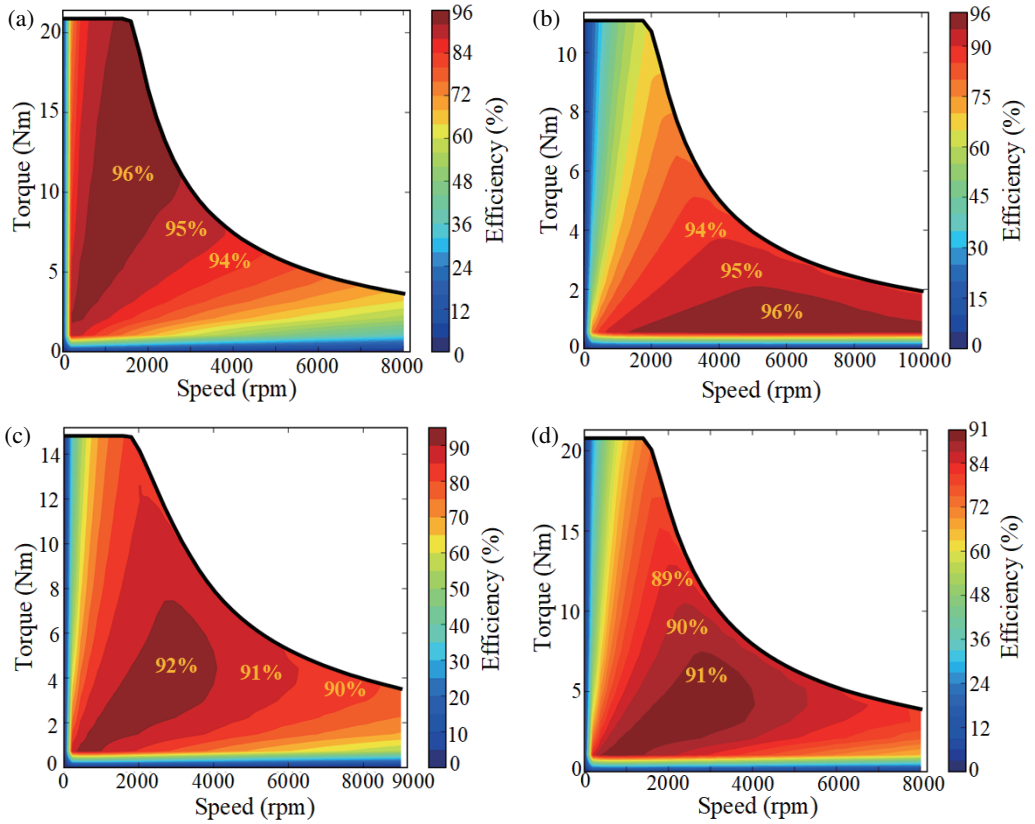

FIGURE 17. Efficiency counter maps with different slot/pole combinations. (a) 12s10p-DL, (b) 12s10p-SL, (c) 12s14p-DL, (d) 12s8p-DL.

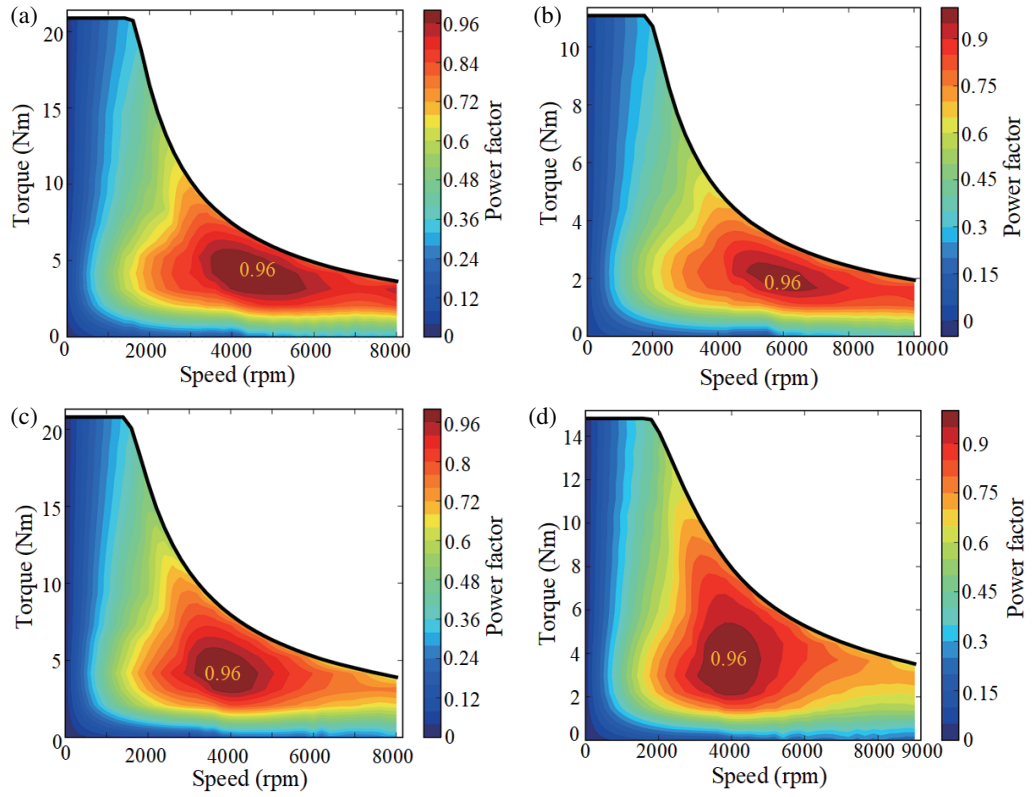

FIGURE 18. Power factor maps with different slot/pole combinations. (a) 12s10p-DL, (b) 12s10p-SL, (c) 12s14p-DL, (d) 12s8p-DL.

In the case of 12s10p-DL as an example, 5 A/mm^2 corresponds to the rated current, which in turn corresponds to a torque of 20.1 Nm. The torque under the overload condition of 12 A/mm^2 is 32.5 Nm, which is 1.61 times of the rated torque. It can be observed that upon the stator core enters the saturated operating section, the machine output torque reaches the maximum value, and then the change tends to level off.

4.6. Efficiency

The efficiency maps of the VFL-PMM with slot and pole combinations at the phase current density 5 A/mm^2 and DC voltage of 140 V are shown in Fig. 17.

The efficiency of the VFL-PMM with 12s10p-DL structure is 96% at rated speed, which gradually decreases with increasing speed and increasing iron loss. The efficiency of the VFL-PMM with 12s10p-SL structure is lower than 12s10p-DL at rated speed. Nevertheless, as the speed increases, a higher efficiency region can be reached in the flux-weakening condition, and the flux-weakening speed can reach 10,000 r/min with efficiency as high as 96%. In contrast to the structure of the 12s10p VFL-PMM, the local high efficiency regions of 12s14-DL and 12s8p-DL are slightly lower. Taking the speed of 3000 r/min and torque of 4 Nm as an example, the efficiency of the 12s14-DL is 92%, and the efficiency of the 12s8p-DL is 91%. Compared to the VFL-PMM with 12s10p structure, the efficiency is lowered by 4.16% and 5.2%, respectively.

4.7. Power Factor

In a permanent magnet machine, if the $i_d = 0$ control strategy is used, its power factor can be calculated as

$$\cos\varphi = \frac{1}{\sqrt{1 + \left(\frac{i_q X_q}{E_{c1} + i_q R}\right)^2}} \tag{8}$$

where ψ is the power factor angle, E_{c1} the amplitude of back EMF, X_q the q-axis armature reactance, i_q the q-axis current, and R the phase resistance.

The variation of the power factor map curves with speed for the slot-pole combinations structure of VFL-PMM is shown in Fig. 18. At the rated operating condition, the power factor is low due to the large L_d. As shown in Equation (8), a larger L_d corresponds to smaller power factor. However, with the increase of speed, the power factor is as high as 0.96 under high speed condition, which solves the problem of low power factor of conventional IPM machines under flux-weakening condition.

5. CONCLUSION

This paper investigates the effect of slot-pole combinations on variable-flux-leakage PM machines. Through certain theoretical analysis and finite element analysis, the conclusions are summarized:

1) Summarize the suitable slot pole combinations for variable flux leakage based on the general rule of FSCW, e.g., 12s10p, 12s8p, 12s14p.

2) The global parametric modeling is used to optimize the split ratio, tooth width, slot depth, and width of the rotor magnetic barrier of the machine. The results show that the machine has the highest PM utilization and efficiency at a split ratio of 0.6.

3) Four types of slot-pole combination structures are analyzed electromagnetically for open-circuit characteristics, cogging torque, torque characteristics, inductance characteristics, variable flux leakage characteristics, overload capacity, efficiency, power factor, and other electromagnetic analyses, to find out the slot-pole combinations that are most suitable for variable flux leakage machines.

4) The VFL-PMM with 12s10p-DL structure produces the largest torque with the smallest torque fluctuation. Moreover, the variable flux range is also the largest, with a variable flux ratio of 12.2%. The efficiency at rated condition is also the highest at 96%. The power factor in the flux-weakening state is 0.96.

ACKNOWLEDGEMENT

This work at Jiangxi University of science and technology was sponsored by the National Natural Science Foundation of China (NNSFC) under Grant Nos. 52067008.

REFERENCES

[1] Gu, X., Z. Zhang, L. Sun, S. Yu, W. Zhang, and L. Yu, "Investigation of a parallel hybrid excitation machine with auxiliary winding for loss reduction in flux-weakening operation," *IEEE Transactions on Transportation Electrification*, Vol. 10, No. 1, 67–77, 2023.

[2] Zhao, Y., D. Li, X. Ren, Z. Liang, and R. Qu, "Low pole-pair ratio integration design of permanent magnet vernier machine with improved power factor," *IEEE Transactions on Industrial Electronics*, Vol. 71, No. 3, 2820–2830, 2023.

[3] Zhou, H. and D. Gerling, "Proposal of torque-correct-by-construction optimization method for axial flux machines," *IEEE Transactions on Energy Conversion*, Vol. 38, No. 3, 1511–1520, 2023.

[4] Xiao, Y., Z.-Q. Zhu, S. S. Wang, G. W. Jewell, J. T. Chen, D. Wu, and L. M. Gong, "A novel asymmetric interior permanent magnet machine for electric vehicles," *IEEE Transactions on Energy Conversion*, Vol. 36, No. 3, 2404–2415, 2021.

[5] Amara, Y., S. Hlioui, H. B. Ahmed, and M. Gabsi, "Power capability of hybrid excited synchronous motors in variable speed drives applications," *IEEE Transactions on Magnetics*, Vol. 55, No. 8, 1–12, 2019.

[6] Morimoto, S., M. Sanada, and Y. Takeda, "Wide-speed operation of interior permanent magnet synchronous motors with high-performance current regulator," *IEEE Transactions on Industry Applications*, Vol. 30, No. 4, 920–926, 1994.

[7] Sneyers, B., D. W. Novotny, and T. A. Lipo, "Field weakening in buried permanent magnet AC motor drives," *IEEE Transactions on Industry Applications*, Vol. IA-21, No. 2, 398–407, 1985.

[8] Limsuwan, N., T. Fukushige, K. Akatsu, and R. D. Lorenz, "Design methodology for variable-flux, flux-intensifying interior permanent magnet machines for an electric-vehicle-class inverter rating," in *2013 IEEE Energy Conversion Congress and Exposition*, 1547–1554, Denver, CO, USA, 2013.

[9] Liu, W., H. Yang, H. Lin, and X. Liu, "Influence of low-coercive-force magnet property on electromagnetic performance of variable flux memory machine," *IEEE Transactions on Magnetics*, Vol. 58, No. 8, 1–6, 2022.

[10] Kato, T., N. Limsuwan, C.-Y. Yu, K. Akatsu, and R. D. Lorenz, "Rare earth reduction using a novel variable magnetomotive force flux-intensified IPM machine," *IEEE Transactions on Industry Applications*, Vol. 50, No. 3, 1748–1756, 2013.

[11] Limsuwan, N., T. Kato, K. Akatsu, and R. D. Lorenz, "Design and evaluation of a variable-flux flux-intensifying interior permanent-magnet machine," *IEEE Transactions on Industry Applications*, Vol. 50, No. 2, 1015–1024, 2013.

[12] Minowa, M., H. Hijikata, K. Akatsu, and T. Kato, "Variable leakage flux interior permanent magnet synchronous machine for improving efficiency on duty cycle," in *2014 International Power Electronics Conference (IPEC-Hiroshima 2014-ECCE ASIA)*, 3828–3833, Hiroshima, Japan, 2014.

[13] Zhu, X., W. Wu, S. Yang, Z. Xiang, and L. Quan, "Comparative design and analysis of new type of flux-intensifying interior permanent magnet motors with different Q-axis rotor flux barriers," *IEEE Transactions on Energy Conversion*, Vol. 33, No. 4, 2260–2269, 2018.

[14] Zhu, X., Y. Zhou, L. Zhang, Z. Peng, and W. Dong, "A fault detection and compensation strategy of the resolver for variable leakage flux permanent magnet motor with threshold self-regulation," *IEEE Journal of Emerging and Selected Topics in Power Electronics*, Vol. 12, No. 3, 3063–3075, 2024.

[15] Zhu, X., L. Xu, L. Li, W.-H. Chen, W. Fan, Z. Jin, and L. Quan, "Current decoupling model predictive control of a leakage flux controllable PM motor in virtual flux reference frame," *IEEE Transactions on Industrial Electronics*, Vol. 71, No. 8, 8471–8481, 2023.

[16] Fan, W., X. Zhu, L. Quan, W. Wu, L. Xu, and Y. Liu, "Flux-weakening capability enhancement design and optimization of a controllable leakage flux multilayer barrier PM motor," *IEEE Transactions on Industrial Electronics*, Vol. 68, No. 9, 7814–7825, 2020.

[17] Zhou, X., X. Zhu, W. Wu, Z. Xiang, Y. Liu, and L. Quan, "Multi-objective optimization design of variable-saliency-ratio PM motor considering driving cycles," *IEEE Transactions on Industrial Electronics*, Vol. 68, No. 8, 6516–6526, 2020.

[18] Wang, C., Z. Zhang, Y. Liu, W. Geng, and H. Gao, "Effect of slot-pole combination on the electromagnetic performance of ironless stator AFPM machine with concentrated windings," *IEEE Transactions on Energy Conversion*, Vol. 35, No. 2, 1098–1109, 2020.

[19] Sun, X., Z. Zhu, S. Cai, L. Wang, F. Wei, and B. Shao, "Influence of stator slot and rotor pole number combination on field winding induced voltage ripple in hybrid excitation switched flux machine," *IEEE Transactions on Energy Conversion*, Vol. 36, No. 2, 1245–1261, 2020.

[20] Li, Y., Z. Q. Zhu, and A. Thomas, "Generic slot and pole number combinations for novel modular permanent magnet dual 3-phase machines with redundant teeth," *IEEE Transactions on Energy Conversion*, Vol. 35, No. 3, 1676–1687, 2020.

[21] Jalali, P., S. T. Boroujeni, and J. Khoshtarash, "Expansion of the feasible slot/pole combinations in the fractional slot PM machines by applying three-slot pitch coils," *IEEE Transactions on Energy Conversion*, Vol. 34, No. 2, 993–999, 2018.

[22] Tessarolo, A., C. Ciriani, M. Bortolozzi, M. Mezzarobba, and N. Barbini, "Investigation into multi-layer fractional-slot concentrated windings with unconventional slot-pole combinations," *IEEE Transactions on Energy Conversion*, Vol. 34, No. 4, 1985–1996, 2019.

[23] Qi, J., Z.-Q. Zhu, G. W. Jewell, L. Yan, C. Gan, Y. Ren, S. Brockway, and C. Hilton, "Influence of slot/pole number combinations and pole shaping on electromagnetic performance of permanent magnet machines with unbalanced north and south poles," *IET Electric Power Applications*, Vol. 17, No. 5, 628–655, 2023.